JOURNAL OF VIROLOGY, Aug. 2008, p. 7264–7275 Vol. 82, No. 15
0022-538X/08/$08.00+0 doi:10.1128/JVI.00737-08

Severe Acute Respiratory Syndrome Coronavirus Infection Causes Neuronal Death in the Absence of Encephalitis in Mice Transgenic for Human ACE2[▽]

Jason Netland,[1] David K. Meyerholz,[2] Steven Moore,[2] Martin Cassell,[3] and Stanley Perlman[1,4]*

Interdisciplinary Program in Immunology[1] and Departments of Pathology,[2] Anatomy and Cell Biology,[3] and Microbiology,[4] University of Iowa, Iowa City, Iowa 52242

Received 3 April 2008/Accepted 12 May 2008

Infection of humans with the severe acute respiratory syndrome coronavirus (SARS-CoV) results in substantial morbidity and mortality, with death resulting primarily from respiratory failure. While the lungs are the major site of infection, the brain is also infected in some patients. Brain infection may result in long-term neurological sequelae, but little is known about the pathogenesis of SARS-CoV in this organ. We previously showed that the brain was a major target organ for infection in mice that are transgenic for the SARS-CoV receptor (human angiotensin-converting enzyme 2). Herein, we use these mice to show that virus enters the brain primarily via the olfactory bulb, and infection results in rapid, transneuronal spread to connected areas of the brain. This extensive neuronal infection is the main cause of death because intracranial inoculation with low doses of virus results in a uniformly lethal disease even though little infection is detected in the lungs. Death of the animal likely results from dysfunction and/or death of infected neurons, especially those located in cardiorespiratory centers in the medulla. Remarkably, the virus induces minimal cellular infiltration in the brain. Our results show that neurons are a highly susceptible target for SARS-CoV and that only the absence of the host cell receptor prevents severe murine brain disease.

Severe acute respiratory syndrome (SARS) first emerged in Guangdong Province, China, in late 2002. By July 2003, when the outbreak was contained, more than 8,000 cases had been reported, with a mortality rate of approximately 10% (35). The etiological agent for SARS was identified as a novel human coronavirus (SARS-CoV) (16, 24, 35, 40). Since there has been only a single significant outbreak of human SARS, most aspects of pathogenesis are poorly understood. While the respiratory tract is clearly the most important site of infection, several other organs, including the brain, have been shown to contain virus or viral products. The role of infection of these other organs in disease outcome is not known and, in the absence of ongoing human disease, can only be addressed with a suitable animal model. SARS-CoV replicates in mice, hamsters, ferrets, and numerous nonhuman primates species, but none of these animals reproducibly develops clinical disease of equivalent severity to SARS in humans (reviewed in references 39 and 46). However, mice transgenic (Tg) for the expression of human angiotensin-converting enzyme 2 (hACE2), the SARS-CoV receptor (29), are extremely susceptible to the virus, with infection of the lungs and brain observed in all mice after intranasal inoculation (32, 50). These mice are readily infectible because murine ACE2 binds SARS-CoV inefficiently (29) and Tg expression of hACE2 provides a higher-affinity cell receptor for the original human strain. In our study, expression of hACE2 was placed under control of the cytokeratin 18 promoter (K18-*hACE2*) (32).

We developed three lines of K18-*hACE2* mice. Infection with SARS-CoV resulted in a rapidly fatal disease in all three lines, with subtle differences in outcome that correlated with transgene copy number and level of hACE2 mRNA. In mice with the highest copy number (lines 1 and 2), mice lost approximately 20% of their body weight before succumbing from day 3 to 5 postinfection (p.i.), whereas in the presence of a lower copy number, disease onset was slightly delayed, and animals died 5 to 7 days p.i. (line 3). In all lines, extensive virus replication was observed in the lungs, with highest viral titers detected at day 1 p.i. Virus also replicated in the lungs of nontransgenic littermates, but peak titers were lower than in infected K18-*hACE2* mice, and virus was cleared more rapidly. Routine pathological examination suggested that infection in Tg mice initiated in the airways. Subsequently, pathological changes including inflammatory cell infiltration, hemorrhage, epithelial cell sloughing, and congestion of alveolar septa were observed in the lungs. In some moribund mice, evidence of aspiration was detected, which made it difficult to delineate cytopathological effects mediated by direct viral infection.

While virus replicated to high levels in the lungs of these Tg mice, extensive virus replication was also detected in the brain (32, 49). Virus was not detected to a significant extent in this organ at day 2 p.i., but by day 4, a large fraction of cells, predominantly neurons, expressed viral antigen. We detected regional differences in the extent of infection, with some areas of the brain, such as the cerebellum, remaining uninfected while others, such as the thalamus, cerebrum, and brainstem, were heavily infected (32). These results were not anticipated because hACE2 expression levels in the brain were no more than 0.1 to 1% of those in the lungs. This extensive brain infection was postulated to be a major factor in the aspiration pneumonia that we observed. While virus was detected in the

* Corresponding author. Mailing address: Department of Microbiology, University of Iowa, BSB 3-712, Iowa City, IA 52242. Phone: (319) 335-8549. Fax: (319) 335-9999. E-mail: stanley-perlman@uiowa.edu.

▽ Published ahead of print on 21 May 2008.

brain in several studies of patients infected during the outbreak of 2002 to 2003 (14, 20, 53), virtually no infected human brains are available for further study, making it difficult to investigate SARS-CoV-induced neurological disease. Therefore, we used SARS-CoV-infected K18-*hACE2* Tg mice to further address aspects of SARS-CoV infection of the brain, including sites of viral entry into the central nervous system (CNS) and factors responsible for a lethal outcome.

MATERIALS AND METHODS

Mice. Mice Tg for expression of hACE2 (K18-*hACE2*) were generated as previously described (32). Pathogen-free C57BL/6 mice were purchased the National Cancer Institute. All animal studies were approved by the University of Iowa Animal Care and Use Committee.

Mouse infections. The Urbani strain of SARS-CoV was obtained from W. Bellini and T. Ksiazek at the Centers for Disease Control, Atlanta, GA. Virus was propagated, and the titer was determined on Vero E6 cells. The titer of virus used for all studies, as determined by plaque assay, was 7.6×10^6 PFU/ml. Mice were lightly anesthetized with isoflurane and infected intranasally with 2.4×10^4 PFU of SARS-CoV in 30 μl of Dulbecco's modified Eagle's medium or intracranially with the indicated doses (see figure legends) of SARS-CoV in 40 μl of Dulbecco's modified Eagle's medium. All work with SARS-CoV was conducted in the University of Iowa BSL3 (biosafety level 3) Laboratory Core Facility. In some experiments, mice were infected intranasally with 5×10^4 to 8×10^4 PFU of the murine CoV, mouse hepatitis virus (MHV) strain JHM (JHMV).

Histology and immunohistochemistry. Animals were anesthetized and transcardially perfused with phosphate-buffered saline followed by zinc formalin. Organs were removed, fixed in zinc formalin, and paraffin embedded. For routine histology, sagittal or coronal sections were stained with hematoxylin and eosin. SARS-CoV viral antigen was detected using a biotin-conjugated monoclonal antibody (MAb) to SARS-CoV N protein (generously provided by John Nicholls, University of Hong Kong), followed by streptavidin-horseradish peroxidase conjugate (Jackson Immunoresearch, West Grove, PA) and diaminobenzidine (Sigma-Aldrich, St. Louis, MO). JHMV viral antigen was detected using a mouse MAb to the N protein (provided by Michael Buchmeier, University of California at Irvine, Irvine, CA) followed by biotin conjugated goat anti-mouse immunoglobulin G (IgG) (Zymed Laboratories, San Francisco, CA), streptavidin-horseradish peroxidase conjugate, and diaminobenzidine.

Scoring of lung pathology. Hematoxylin- and eosin-stained lung sections were assessed using the scoring system described in the figure legends. Three animals for each time point were analyzed.

Neuronal counting. Eight-micrometer brain sections were stained with cresyl violet. Neurons were quantified by manually counting cells with visible nucleoli in a blinded fashion, as previously described (12). For each region of the brain, three adjacent fields were counted at ×40 magnification and averaged. A total of four infected and four uninfected age-matched mice were analyzed.

TUNEL assay. Terminal deoxynucleotidyltransferase-mediated dUTP-biotin nick end labeling (TUNEL) staining was performed using an In Situ Cell Death Detection Kit (Roche, Indianapolis, IN) according to the manufacturer's instructions.

Confocal microscopy. Immunofluorescence staining was performed as previously described (23). Briefly, fixed, paraffin-embedded sections were deparaffinized and hydrated. Sections were permeabilized with 0.1% Triton X-100, blocked with 10% horse serum, and incubated sequentially with primary antibody overnight at 4°C and secondary antibody for 1 h at room temperature. The following primary antibodies were used: rabbit anti-mouse glial fibrillary acidic protein (GFAP) (DAKO, Carpinteria, CA), rabbit anti-mouse Iba1 (ionized calcium-binding adaptor molecule 1) (Wako Chemicals USA, Richmond, VA), goat anti-mouse interleukin-6 (IL-6) (R&D Systems, Minneapolis, MN), mouse anti-MHV N and fluorescein isothiocyanate (FITC)-conjugated anti-SARS-CoV N. Secondary antibodies utilized were Cy3-conjugated donkey anti-goat IgG, FITC-conjugated donkey anti-rabbit IgG, Cy3-conjugated donkey anti-mouse IgG, or FITC-conjugated donkey anti-mouse IgG (all purchased from Jackson Immunoresearch). Microscopy was conducted on a Zeiss LSM 510 Confocal Microscope (Carl Zeiss MicroImaging, Thornwood, NY).

Statistical analysis. A Student's *t* test was used to analyze differences in mean values between groups. All results are expressed as means ± standard errors of the means. *P* values of <0.05 were considered statistically significant.

RESULTS

SARS-CoV infects airways and alveoli of K18-*hACE2* mice but causes limited pathology. Although our prior study suggested that infection of the brain was the major contributory factor in a fatal outcome, we also detected changes in the lungs consistent with aspiration, present only in K18-*hACE2* mice at day 4 p.i., that hampered efforts to determine the importance of pulmonary infection in disease. Consequently, we initiated an additional set of studies examining a more complete time course of infection in both Tg and non-Tg animals. Our initial studies used hACE2 Tg mice that were generated on a $(C57BL/6 \times SJL/J)F_2$ background and were crossed two to three times to C57BL/6 mice (32). Since then, we have backcrossed the mice an additional five to six times to B6 mice, without observing any changes in susceptibility to SARS-CoV infection. For the studies described in this report, we used only animals from a single line (line 3), the line that exhibited the most prolonged disease time course, with mice surviving until days 5 to 7 p.i. We sacrificed intranasally inoculated Tg mice on a daily basis at days 1 to 6 p.i. Mice began to die by day 5 p.i., and about 30% of mice survived to day 6 p.i. Using a biotin-conjugated anti-SARS-CoV nucleocapsid protein MAb, we confirmed the presence of viral antigen in the conducting airway epithelia of both K18-*hACE2* mice and non-Tg controls at days 1 and 2 p.i. (Fig. 1A to D and G), with antigen clearance from these sites in both groups of mice by day 3 (Fig. 1G). In our initial study, lungs past day 2 p.i. were not examined for virus antigen. Therefore, using these newly generated samples, we showed that viral antigen was detected in the alveoli of K18-*hACE2* but not non-Tg mice, with maximal levels observed at day 4 p.i. (Fig. 1E, F, and H) before declining at later times (Fig. 1H).

Histological examination of lungs showed mild pathological changes at early times p.i. At day 1 p.i., there was scant evidence of inflammation but a subtle increase in cell bulging/sloughing into the airways in both K18-*hACE2* and non-Tg mice (Fig. 2A and I). Starting at day 2, we detected similar amounts of peribronchiolar inflammation and proliferation in both types of mice (Fig. 2B, C, J, and K). In contrast, interstitial disease, characterized by perivascular and septal cellular infiltration, edema, and congestion, was detected in all K18-*hACE2* but not non-Tg mice (Fig. 2D). We also detected intense neutrophilic infiltrates in the airways of all K18-*hACE2* mice sacrificed later than day 4 p.i. (Fig. 2E), in agreement with our previous results (32). Some affected airways contained foreign debris (Fig. 2F), supporting the conclusion that these infiltrates resulted from aspiration. While some of the interstitial disease observed in K18-*hACE2* mice may result from aspiration, some areas of interstitial disease nearly completely overlapped with sites of virus replication (Fig. 2G and H), suggesting that lung disease resulted at least partly from direct virus infection.

Neuronal infection is the major cause of death in K18-*hACE2* mice. To more definitively distinguish between the contributions of lung versus brain infection to a lethal outcome in K18-*hACE2* mice, we inoculated mice intracranially with high (3.2×10^4 PFU) and low (3.2 or 320 PFU) doses of SARS-CoV. Mice infected intracranially at all doses became moribund by day 4 p.i. Infection with 3.2×10^4 PFU resulted in a

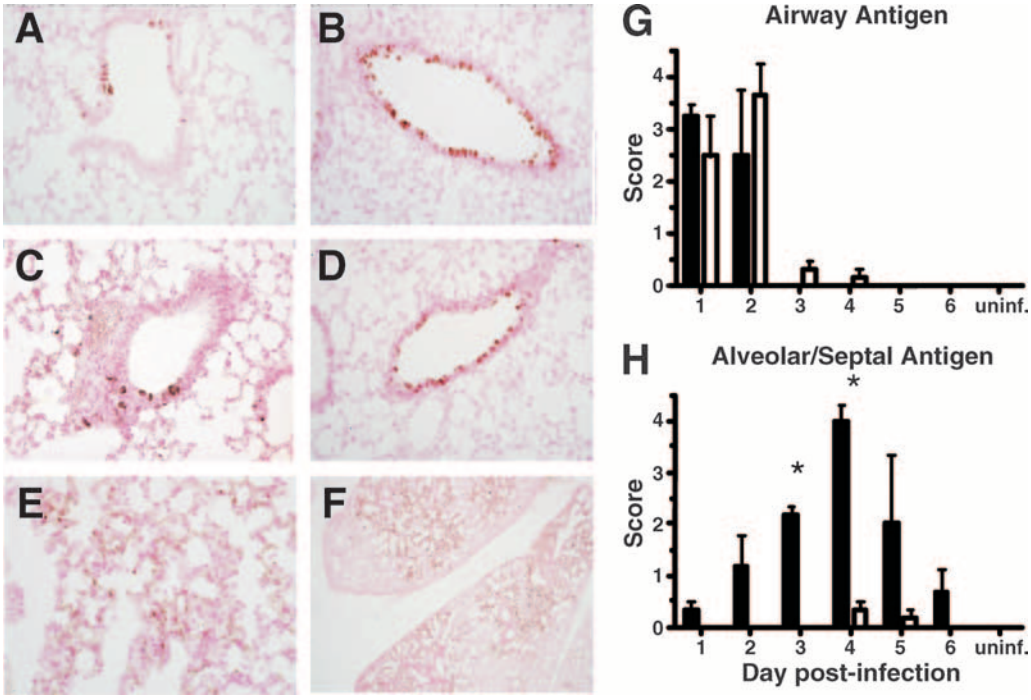

FIG. 1. SARS-CoV antigen staining in the lungs of K18-*hACE2* Tg and wild-type mice. K18-*hACE2* Tg (A, C, E, and F) and non-Tg (B and D) mice were infected intranasally with 2.4×10^4 PFU of SARS-CoV (Urbani strain). Three mice from each group were sacrificed at days 1 to 6 p.i. Lungs were harvested, fixed, sectioned, and stained with anti-SARS-CoV N protein MAb. Viral antigen was localized to the conducting airway of Tg and non-Tg mice at day 1 (A and B) and day 2 p.i. (C and D). Antigen was detected in the alveoli at day 4 p.i (E and F). (G and H) Scoring of antigen staining in the airway and in alveoli. Airway antigen was scored by determining the percentage of infected airways; alveolar staining was scored based on the percentage of lung that was infected. In both cases, the scoring is as follows: 0, 0%; 1, 10 to 20%; 2, 30 to 40%; 3, 50 to 60%; 4, 70 to 80%; 5, 90 to 100%. *, $P < 0.05$. Original magnifications: ×20 (A to E) and ×2 (F). uninf, uninfected.

pattern of widespread neuronal infection similar to that observed following intranasal inoculation (Fig. 3A; see also Fig. 4B). Histological examination of the lungs revealed intense neutrophilic infiltrates (Fig. 3B and C) in six of seven cases, with foreign debris/bacteria present in five cases, suggestive of aspiration pneumonia. Low titers of infectious virus were present (Fig. 3G), but we were not able to detect viral antigen in the lungs (Fig. 3C). By contrast, after inoculation with 3.2 or 320 PFU of SARS-CoV, we detected viral antigen throughout the brain (Fig. 3D), although the extent of infection was much less than observed after intranasal or high-dose intracranial inoculation (Fig. 3A; see also Fig. 4B). Unlike mice inoculated intracranially with 3.2×10^4 PFU of SARS-CoV, the lungs appeared normal in all but one of four mice examined (Fig. 3E and F). In this single animal, we observed evidence of mild aspiration (data not shown). As in mice inoculated intracranially with 3.2×10^4 PFU, we detected no viral antigen in the lungs but did detect virus by plaque assay (Fig. 3G). Collectively, these results suggest that SARS-CoV-infected K18-*hACE2* mice die primarily as a direct result of CNS, not pulmonary, infection. They also suggest that the airway infiltrates detected in moribund mice are a complication of the brain infection, occur only after extensive neuronal infection, and are not required for a lethal outcome.

As the low-dose intracranially inoculated animals exhibited limited viral antigen distribution but still rapidly succumbed to infection, we reasoned that neurons in a vital region of the brain would be infected. Examination of brain sections from mice inoculated with 3.2 or 320 PFU of SARS-CoV revealed that the dorsal vagal complex (nucleus tractus solitarii, area postrema, and dorsal motor nucleus of the vagus), critical for cardiorespiratory function, was infected in all four samples examined (Fig. 3H). We also examined brains from mice inoculated intracranially (Fig. 3I) or intranasally (Fig. 3J) with high doses of virus and observed that the dorsal vagal complex was infected in all instances. Thus, the fulminant disease occurring in SARS-CoV-infected K18-*hACE2* mice may result from infection and functional impairment of this critical brain region.

SARS-CoV spreads in the brain of K18-*hACE2* mice transneuronally primarily from the olfactory bulb and induces neuronal loss. The widespread distribution of viral antigen in the brains of intranasally infected K18-*hACE2* mice and the temporal pattern of disease led us to postulate previously that infection occurred via hematogenous spread following lung infection (32). However, from these initial experiments, we could not distinguish transneuronal spread from one or more sites of entry into the CNS from blood-borne spread. To evaluate the kinetics and spread of the neuronal infection, as well as determine the site of entry, we harvested brains from infected animals at days 1 to 6 p.i. Immunohistochemical staining for the SARS-CoV N protein revealed no detectable viral antigen at day 1 or 2 p.i. Viral antigen was first detectable and surprisingly widespread at day 3 p.i. (Fig. 4B). By day 4, we detected virus throughout the brain (Fig. 4C). In mice surviving beyond day 4, viral antigen remained widespread, but small

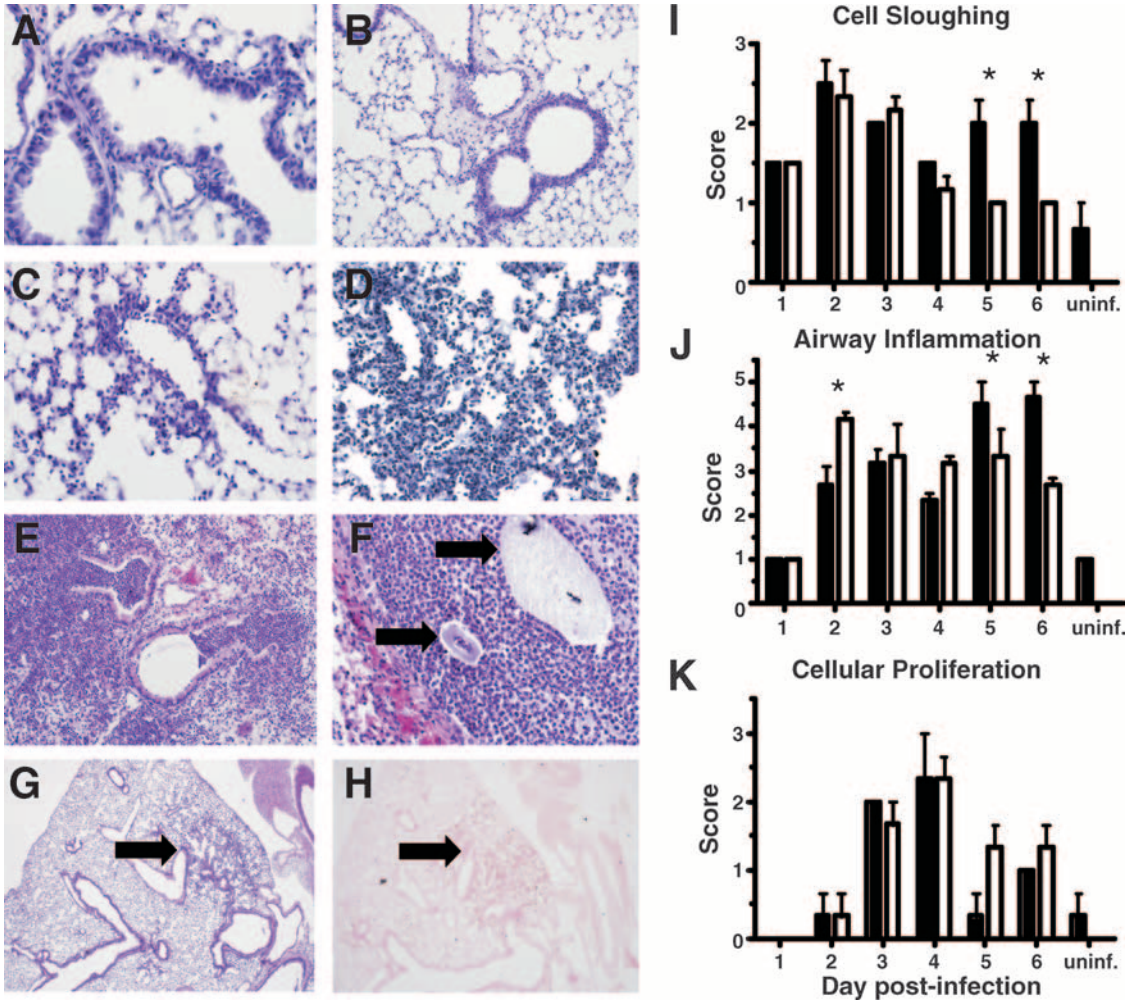

FIG. 2. Lung pathology in SARS-CoV-infected K18-*hACE2* Tg and non-Tg mice. Lungs were harvested from K18-*hACE2* Tg (A, B, and D to H) and non-Tg (C) mice daily from days 1 to 6 p.i., fixed, sectioned, and stained with hematoxylin and eosin. (A) Epithelial cell sloughing from the airway of a Tg animal at day 1 p.i. (B and C) Peribronchial inflammation in both Tg (B) and non-Tg (C) mice at day 2 p.i. (D) Interstitial infiltrates in Tg mouse at day 3 p.i. (E and F) Lungs from Tg mice exhibited intense neutrophilic infiltrates at day 4 p.i. (E) with foreign debris present in many lesions (F, arrows), consistent with aspiration pneumonia. (G and H) Staining of adjacent sections shows that inflammation (G) and SARS-CoV antigen (H) overlap in some regions of the lung (arrows). (I to K) Lungs from three Tg and three non-Tg mice at each day p.i. were scored for cell sloughing (I), airway inflammation (J), and cellular proliferation (K). Cell sloughing scores were based on the number of sloughed/necrotic cells per airway as follows: 0, none detected; 1, rare; 2, 1 to 3; 3, 4 to 6; 4, 7 to 9; and 5, 10 or more. Inflammation scores were assigned as follows: 1, uncommon individual cells; 2, detectable peribronchiolar/perivascular aggregates; 3, moderate cellular aggregates; 4, cellular aggregates with vascular margination; 5, cellular aggregates with vascular margination and edema or alveolar cellular infiltration. Proliferation was scored based on the number of mitotic figures per lung section as follows: 0, no mitotic figures; 1, rare; 2, 2 to 3; 3, 4 to 6; 4, 7 to 9; 5, 10 or more. *, $P < 0.05$. Original magnifications: ×40 (A, C, D, and F), ×20 (B and E), and ×4 (G and H).

areas in which virus appeared to be cleared became evident (Fig. 4D). These regions of virus clearance were the first ones to be infected, and, as shown below, clearance was accompanied by neuronal loss.

Virus spread rapidly within the brain between days 2 and 3 following intranasal inoculation, making it difficult to determine the initial sites of infection. To determine sites of virus entry, we stained sagittal and coronal sections for viral antigen, using brains harvested at 6-h intervals from 48 to 72 and at 96 h p.i. Virus antigen was first detected at 60 to 66 h (Fig. 4A) p.i. and was most abundant in the olfactory bulb. Regions of the cortex (piriform and infralimbic cortices), basal ganglia (ventral pallidum and lateral preoptic regions), and midbrain (dorsal raphe) were also heavily infected; these regions all have first- or second-order connections with the olfactory bulb. Other areas, such as the parataenial nucleus of the thalamus, paraventricular nucleus of the hypothalamus, and the medial and basolateral amygdala, were also virus antigen positive but less consistently (Table 1). This pattern of antigen distribution is strongly suggestive of entry via the olfactory nerve with subsequent transneuronal spread. Examination of brains harvested from mice at day 3 p.i. reinforced this notion. In these samples, antigen was much more widespread but was largely restricted to first- and second-order connections of the olfactory bulb. By day 4 p.i., nearly all regions of the brain stained positive for SARS-CoV antigen with the exception of the ven-

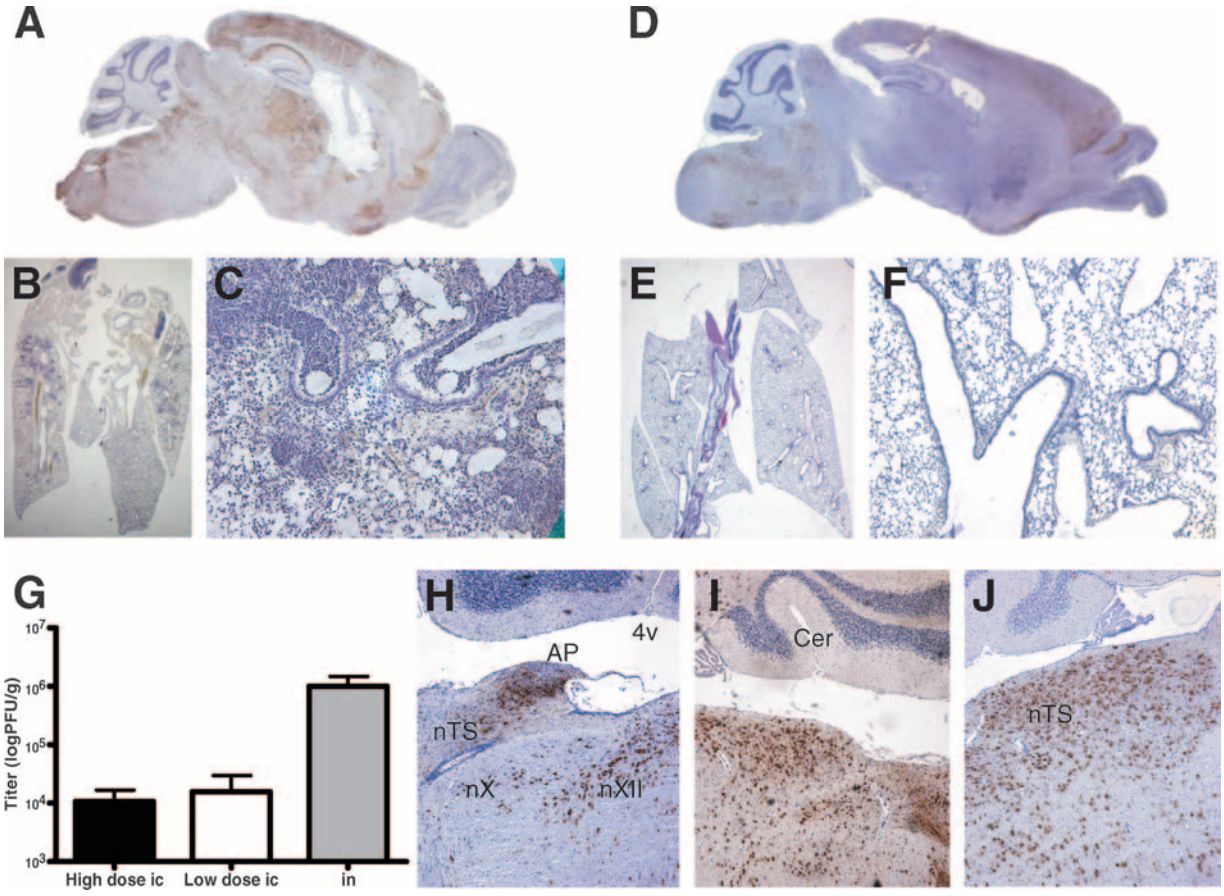

FIG. 3. Intracranial infection of K18-*hACE2* mice with different dosages of SARS-CoV. Tg mice were intracranially inoculated with 3.2×10^4 (high dose) (A-C) or 320 (low dose) (D to F) PFU of SARS-CoV, and lungs and brains were harvested at day 4 p.i. Tissue was fixed, sectioned, and stained for SARS-CoV antigen and with hematoxylin. (A) Viral antigen was detected throughout the brain after infection with 3.2×10^4 PFU of SARS-CoV. (B and C) Aspiration pneumonia was detected in the lungs of animals infected with 3.2×10^4 PFU in the absence of viral antigen ($n = 7$). (D) The distribution of viral antigen in the brains of animals infected with 320 PFU was limited. (E and F) Lungs of mice inoculated with 320 PFU of SARS-CoV showed no evidence of aspiration pneumonia or viral antigen ($n = 4$). (G) Viral titers in the lungs of Tg-positive mice after intracranial or intranasal (2.4×10^4 PFU) virus inoculation at day 4 p.i. ($n = 3$ for all groups) (H to J) Viral antigen is detected in the dorsal vagal complex in mice inoculated at low dose intracranially (H), high dose intracranially (I) and intranasally (J). nT, nucleus tractus solitari; AP, area postrema; nX, dorsal motor nucleus of the vagus; nXII, motor hypoglossal nucleus; 4v, fourth ventricle; Cer, cerebellum. Original magnifications: ×1 (A, B, and E), ×40 (C and F), ×2 (D), and ×5 (H to J).

tral anterior olfactory nucleus, the dentate gyrus, and the cerebellum.

While a number of the areas infected by day 4 p.i. were consistent with spread along olfactory connections, many infected sites were not connected directly with the olfactory bulb. Some of these regions, such as the dorsal vagal complex, nucleus ambiguus, and hypoglossal nucleus, suggested infection via oral uptake, whereas infection of other sites, such as the cochlear nuclei, substantia nigra, and temporal and occipital cortices could not be explained by either olfactory or oral entry/spread. To further assess the role of oral uptake in infection of the CNS, we assayed the small intestine and colon for virus antigen in enterocytes and associated nerve plexuses at day 4 p.i. However, we could not detect viral antigen anywhere in the gut of two infected mice (data not shown), raising the possibility that once virus is established in the brain, it spreads along specific neurotransmitter pathways (such as the serotoninergic dorsal raphe system) that innervate large portions of the brain, or the virus spreads via nonneuronal routes, such as the blood or the Virchow-Robin spaces (13, 52).

Rapid spread throughout the brain appeared to be accompanied by virus clearance at sites of initial infection and concomitant neuronal loss. To assess neuronal loss more precisely, we quantified the number of neurons in several regions of the brain at day 4 p.i. Areas that were infected at earlier times p.i., such as the cingulate and infralimbic cortices and anterior olfactory nucleus exhibited significantly fewer neurons per square millimeter (P values of 0.005, 0.00002, and 0.00006, respectively) than were found in uninfected animals (Fig. 5A). As controls, the numbers of neurons in the dentate gyrus of the hippocampus and deep cerebellar nuclei were quantified, as these structures represent brain regions that were not heavily infected until relatively late times p.i. or that remained largely uninfected. In these regions, neuronal counts were nearly identical in infected and uninfected brains, suggesting that SARS-CoV directly induced neuronal death.

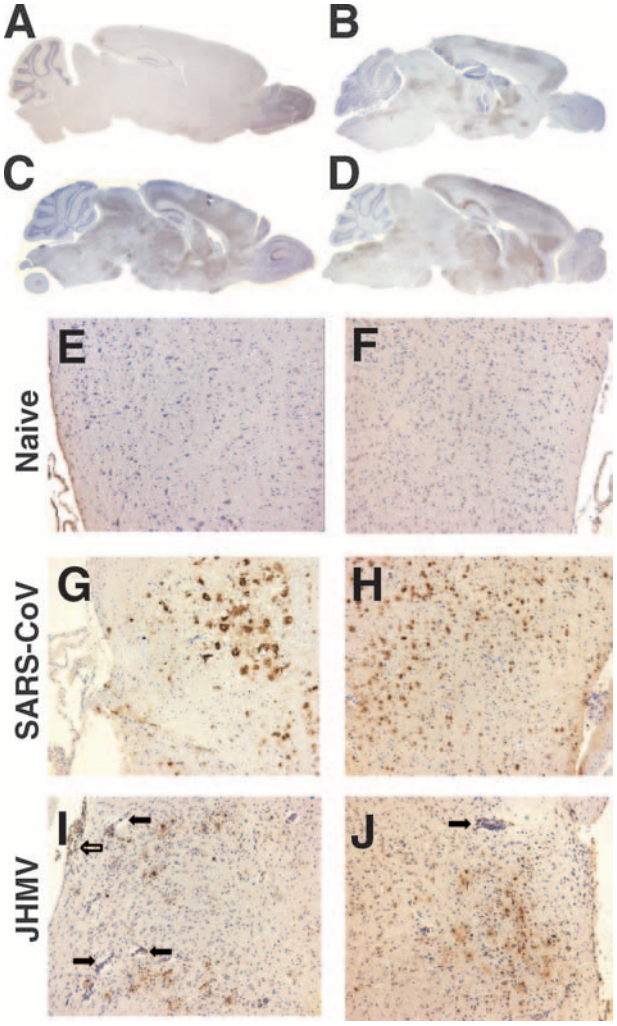

FIG. 4. Viral antigen distribution in the brain following intranasal inoculation. Brains were harvested from mice infected intranasally with 2.4×10^4 PFU and stained for viral antigen. (A to C) Antigen distribution in the brain at 60 h (A) and 3 (B), 4 (C), and 5 (D) days p.i. (E to J) The brain stem (E, G, and I) and hypothalamus (F, H, and J) were examined for viral antigen and inflammation. (E and F) Naïve controls. (G and H) SARS-CoV-infected brains exhibited antigen exclusively in neurons with no obvious inflammation at day 6 p.i. (compare to naïve controls). (I and J) JHMV-infected brains showed less extensive neuronal infection but severe perivascular inflammation (closed arrows) and meningitis (open arrows) at day 6 p.i. Original magnifications: ×1 (A to D) and ×5 (E to J).

Minimal signs of inflammation are detected in infected K18-*hACE2*-infected brains. No evidence of inflammation was detected in the brains of any infected K18-*hACE2* mice even when infection was widespread (Fig. 4G and H), and these brains were virtually indistinguishable from uninfected brains (Fig. 4E and F). For comparison, we also examined brains harvested from mice infected with another group 2 CoV, JHMV, which is highly neurotropic and induces extensive cellular infiltration. As expected, JHMV-infected brains displayed perivascular inflammation (Fig. 4I and J, closed arrows) and meningitis (open arrow) when examined at day 6 p.i. The lack of inflammation in SARS-CoV-infected brains raised the possibility that neurons died by apoptosis, a form of cell death associated with minimal cellular infiltration. Therefore, we assayed cells for apoptosis by performing TUNEL staining at days 1 to 6 p.i. TUNEL-positive cells were not detected in any of the SARS-CoV-infected brains (Fig. 5D and E) but were readily detected in DNase 1-treated uninfected brain sections (Fig. 5B and C). Thus, apoptotic death of neurons does not explain the lack of inflammation that we observed.

Another consequence of inflammation in the CNS is activation of astrocytes and microglia and migration to areas of infection, where they exert numerous effector functions involved in pathogen clearance, modulation of the immune response, and tissue repair (reviewed in references 3 and 15). To examine changes in the activation and location of microglia and astrocytes, we costained tissue sections from infected brains with anti-SARS-CoV N antibody and antibodies directed against GFAP or Iba1, which stain astrocytes and microglia/macrophages, respectively. GFAP expression by astrocytes was detected in limited areas in SARS-CoV-infected animals with a distribution and intensity of staining similar to that observed in naïve animals (Fig. 6A). In contrast, JHMV-infected brains displayed upregulation of GFAP, and the GFAP-positive cells were found throughout the brain. These findings suggest that astrocytes in SARS-CoV-infected mice were not activated, despite extensive neuronal infection. However, we did observe similar numbers of Iba1-positive cells in the brains of SARS-CoV and JHMV-infected animals at day 6 p.i. while very few were detected in naïve controls (Fig. 6B).

While the cellular response to SARS-CoV in the brains of K18-*hACE2* mice was minimal, proinflammatory cytokines and chemokines are upregulated in the brains of infected mice at day 4 p.i. (32, 49). In JHMV-infected mice and in other CNS infections, cytokines are generally expressed by glia and infiltrating cells, especially astrocytes and macrophages (3, 42, 47). In general, these cytokine-producing cells are uninfected, and cytokines are expressed as part of the proinflammatory response. To determine the cellular source for these cytokines, we examined the localization of a representative cytokine, IL-6, which is highly upregulated in SARS-CoV-infected brains and has both protective and immunopathological roles in the inflamed CNS (9, 34). Abundant amounts of IL-6 were detected in infected brains (Fig. 7A). Astrocytes are known to be a major site of IL-6 synthesis under conditions of inflammation (17), and consistent with this, some of the IL-6-expressing cells were uninfected astrocytes. In contrast, however, the majority of cells that produced IL-6 were SARS-CoV infected and were morphologically neurons. As a control, we showed that although occasional neurons stained positive for IL-6, astrocytes were the major source of IL-6 in the brains of JHMV-infected mice (Fig. 7B).

DISCUSSION

While SARS-CoV is considered a respiratory pathogen in humans, the virus has been detected in the brains of infected patients. In one report, examination of autopsy samples from eight patients with SARS revealed the presence of SARS-CoV in brain samples by immunohistochemistry, electron microscopy, and real-time reverse transcription-PCR (20). In another study, using immunohistochemistry and in situ hybridization,

TABLE 1. Viral antigen distribution in the brains of K18-*hACE2* mice

Brain region[a]	Distribution of antigen at the indicated time p.i.[b]		
	60–66 h	Day 3	Day 4
Cerebellum			
Purkinje cells	−	−	+
Granule cells	−	−	−
Deep nuclei	−	−	(+)
Medulla			
Parvicellular RF	(+)	+	+++
Nucleus solitary tract	−	(+)	++
Cuneate nucleus	−	−	(+)
External cuneate nucleus	−	−	++
Medial vestibular nucleus	−	−	+
Reticular giganto	−	−	+
Nucleus ambiguus	−	−	+
Spinal V caudal	−	−	−
Intermediate	−	−	(+)
Rostral	−	−	−
Rostroventral (RVLM)	−	−	+
Lateral paragigant nucleus	−	+	++
Nucleus XII	−	+	++
Nucleus X	−	+	++
Dorsal cochlear nucleus	−	−	++
Ventral cochlear nucleus	−	−	(+)
Pons			
Nucleus VII	−	−	++
Nucleus prepositus	−	−	++
Inferior olive nucleus	−	−	+
Pontine nuclei	−	−	++
Lateral parabrachial nucleus	−	++	++
Medial parabrachial nucleus	−	+	+
Lateral parabrachial nucleus	−	+	+
Midbrain			
Mesencephalic V	−	+	+
Nucleus pontis oralis	−	−	−
Inferior colliculus	−	−	++
Superior colliculus	−	−	++
PPT	−	−	(+)
Lateral dorsal tegmental nucleus	−	+	++
Periaqueductal gray	−	+	+++
Dorsal raphe	+	+++	++
Red nucleus	−	−	+
Substantia nigra, pr	−	+	+++
Substantia nigra, pc	−	−	(+)
Thalamus			
VPL nucleus	−	+	+++
VPM nucleus	−	++	+++
VA/VL nucleus	−	++	+++
Mediodorsal	−	++	+++
Midline	(+)	++	+++
Reticular	−	+	++
Laterodorsal	−	+	+++
Medial geniculate	−	++	+++
Lateral geniculate	−	++	++
Posterior	−	+	+++
Hypothalamus			
Ventromedial	−	+++	++
Lateral	−	++	++
Posterior	−	++	++
Arcuate	−	++	+
Suprachiasmatic	−	+++	++
Paraventricular	(++)	+++	+++
Supraoptic	−	++	++
Medial preoptic	(+)	+++	++
Subfornical organ	−	+	++
Amygdala			
Basolateral	(+)	(+)	+++
Lateral	−	(+)	+++
Central	−	−	+
Periamygdala cortex	−	−	+++
Medial	(+)	+	+
Posterior group	−	+	+++
Anterior cortical	−	++	+++
Hippocampus			
CA1-4	−	−	+++
Dentate gyrus	−	+	+++
Medial septum	(+)	++	+++
Lateral septum	−	−	+
Subiculum	−	+	+++
Basal ganglia			
Caudate-putamen	−	−	+++
Globus pallidus	−	(+)	++
Ventral pallidum	+(+)	+++	++
Lateral preoptic	+(+)	+++	++
Nucleus accumbens	(+)	+++	++
Fundus striati	−	++	+++
Olfactory tubercle	(+)	+++	+++
Cortex			
Frontal	−	+	+++
Infralimbic	+	+++	+
Prelimbic	−	−	+(+)
Lateral orbital	+(+)	++	++
Cingulate	(+)	++	+(+)
Parietal	−	(+)	+++
Retrosplenial	−	−	+
Temporal	−	−	++
Occipital	−	−	+
Perirhinal	−	(+)	(+)
Entorhinal	(+)	++	+++
Insula, granular	−	+	+++
Dysgranular	−	+	++
Agranular	(+)	++	+++
Piriform	+	++	+++
Olfactory bulb			
AON, dorsal	(+)	+++	++
AON, medial	−	−	+
AON, lateral	+	+	+
AON, ventral	−	−	−
Taenia tecta	+	+++	(+)
Mitral cells	+	++	+++
IPL		−	−
EPL		−	−
Inner gran		−	+

[a] Abbreviations: RF, reticular formation; RVLM, rostral ventrolateral medulla; PPT, pendunculopontine tegmental nucleus; pr, pars reticulate; pc, pars compaacta; VPL, ventral posterolateral; VPM, ventral posterior medial; VA, ventroanterior; VL, ventrolateral; AON, anterior olfactory nucleus; IPL, inferior parietal lobe. Brain regions are as described by Paxinos and Franklin (34a).

[b] −, no antigen detected; +, 1 to 5 positive cells/structure; ++, 6 to 20 positive cells/structure; +++, >20 cells/structure. (+), antigen was not detected in all samples analyzed.

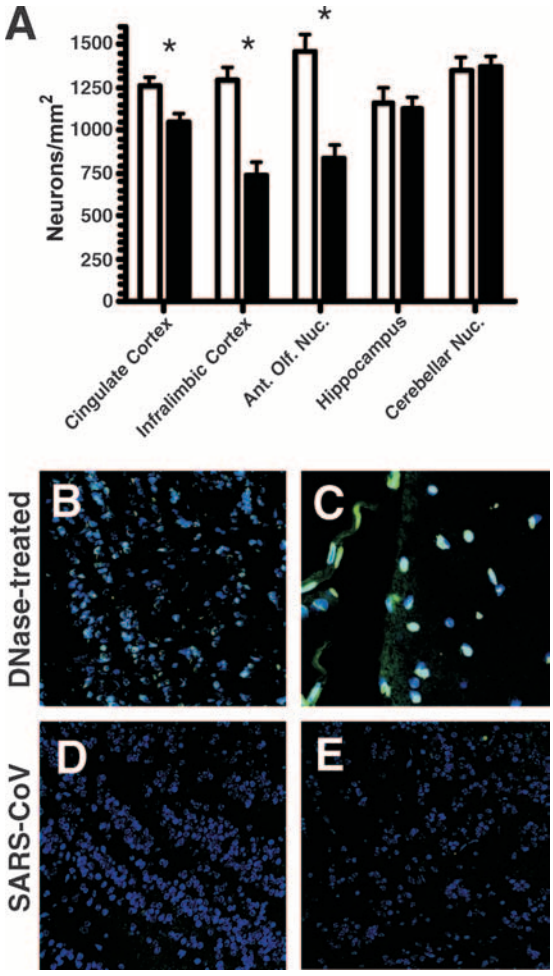

FIG. 5. Infection results in neuronal death but does not induce apoptosis. (A) Brain sections from age-matched uninfected ($n = 4$) (white bars) mice and mice at day 4 p.i. ($n = 4$) (black bars) were stained with cresyl violet, and the number of neurons in the indicated regions were quantified by light microscopy. For each region, three adjacent fields were counted and averaged. Infected mice showed a significant reduction in neurons in the cingulate cortex, infralimbic cortex, and anterior olfactory nucleus (Ant Olf Nuc) compared to uninfected controls. No difference was detected in the hippocampus and cerebellar nucleus (Nuc). *, $P < 0.005$. (B to E) Brain sections from infected (D and E) and DNase-treated uninfected mice (B and C) were assayed for apoptosis by TUNEL assay. TUNEL-positive cells (green) were detected in DNase 1-treated brains (B and C) but were not present in SARS-CoV-infected brains at either day 4 (D) or day 6 (E). Nuclei were labeled with TOPRO-3 (blue). Original magnification, ×40 for all images.

Ding et al. detected virus in the cerebrum (but not the cerebellum) in four SARS cases (14). Furthermore, some patients who survived SARS display neurological/psychological sequelae that appear to be disproportionate to the extent of lung infection or expected side effects of corticosteroid therapy (11, 25, 28, 53) (steroids were used in most patients with SARS in the outbreak of 2002 to 2003) (45). In one such patient with neurological sequelae, SARS-CoV was detected in the cerebrospinal fluid by reverse transcription-PCR during the acute phase of illness (25). In another instance, Xu et al. described a patient who developed progressive neurological symptoms starting at day 28 after onset. This patient later succumbed to infection, and autopsy revealed the presence of SARS-CoV in the brain accompanied by neuronal necrosis, glial hyperplasia, and edema (53). Our results are consistent with the notion that direct infection of the human CNS occurs in some patients.

In all studies that examined brain sections from SARS patients, virus was detected almost exclusively in neurons (14, 20, 53), consistent with studies showing a marked neuronal tropism in infected *hACE2* Tg mice (32, 49). Further, human neural cells, including neurons, are infectible by SARS-CoV (54), and neuronal expression of ACE2 has been detected in the human CNS (21). Infection of neurons was also observed in C57BL/6 mice infected intranasally with SARS-CoV at late times after infection and in mice infected with a mouse-adapted strain of SARS-CoV (19, 38, 49). Tg expression of hACE2, while not resulting in high-level expression (32), is sufficient to facilitate overwhelming neuronal infection. These results are consistent with the well-described propensity of other CoVs to infect CNS cells in general and neurons specifically. Human CoVs (HCoV)-OC43 and HCoV-229E, which primarily cause the common cold, are also detected in the human brain (4), and animal viruses such as MHV, bovine CoV, and mouse-adapted strains of HCoV-OC43 readily infect the murine CNS, causing neuronal infections (1, 7, 22, 31).

Our results suggest that SARS-CoV primarily entered the brain via the olfactory nerve. However, the rate at which SARS-CoV spread within the brain was striking. Viral antigen was not detected until 60 to 66 h p.i. and, by this time, was already present in the olfactory bulb and several brain regions connected to this structure. Furthermore, 6 to 12 h later, viral antigen was detected throughout the brain and had spread to first- and second-order structures connected with the olfactory bulb as well as structures only remotely connected with the olfactory system. This is in contrast to other viral infections in the murine brain where spread from the olfactory bulb to directly connected sites takes approximately 1 day, with spread to more distal sites taking an additional several days (5, 6, 26, 37). One explanation for this rapid spread is that the replicative cycle of SARS-CoV is short. This possibility is supported by in vitro studies in which production of new virus particles was detected as early as 3 to 5 h p.i. (33, 44). Alternatively, virus load in initial sites of infection may be sufficiently high so that virus is able to spread transneuronally to distally connected neurons without a requirement for replication in all infected cells along a pathway. Virus may also spread along the Virchow-Robin spaces surrounding arterioles and venules, as has been demonstrated for a number of other neurotropic pathogens (13, 52).

Several mechanisms may explain how brain infection leads to death in SARS-CoV-infected K18-*hACE2* mice. While widespread neuronal infection and dropout are likely to contribute to severe disease, the level of neuronal infection is modest in mice inoculated intracranially with low doses of virus compared to those infected intranasally or with high dosages intracranially. However, infection of the cardiorespiratory center in the medulla is observed even when mice receive only low doses of SARS-CoV intracranially (Fig. 3D and H) and could contribute to the death of the animal. It is also possible that excessive levels of proinflammatory cytokines/chemokines in the brain result in a "cytokine storm" and lethal disease. It is

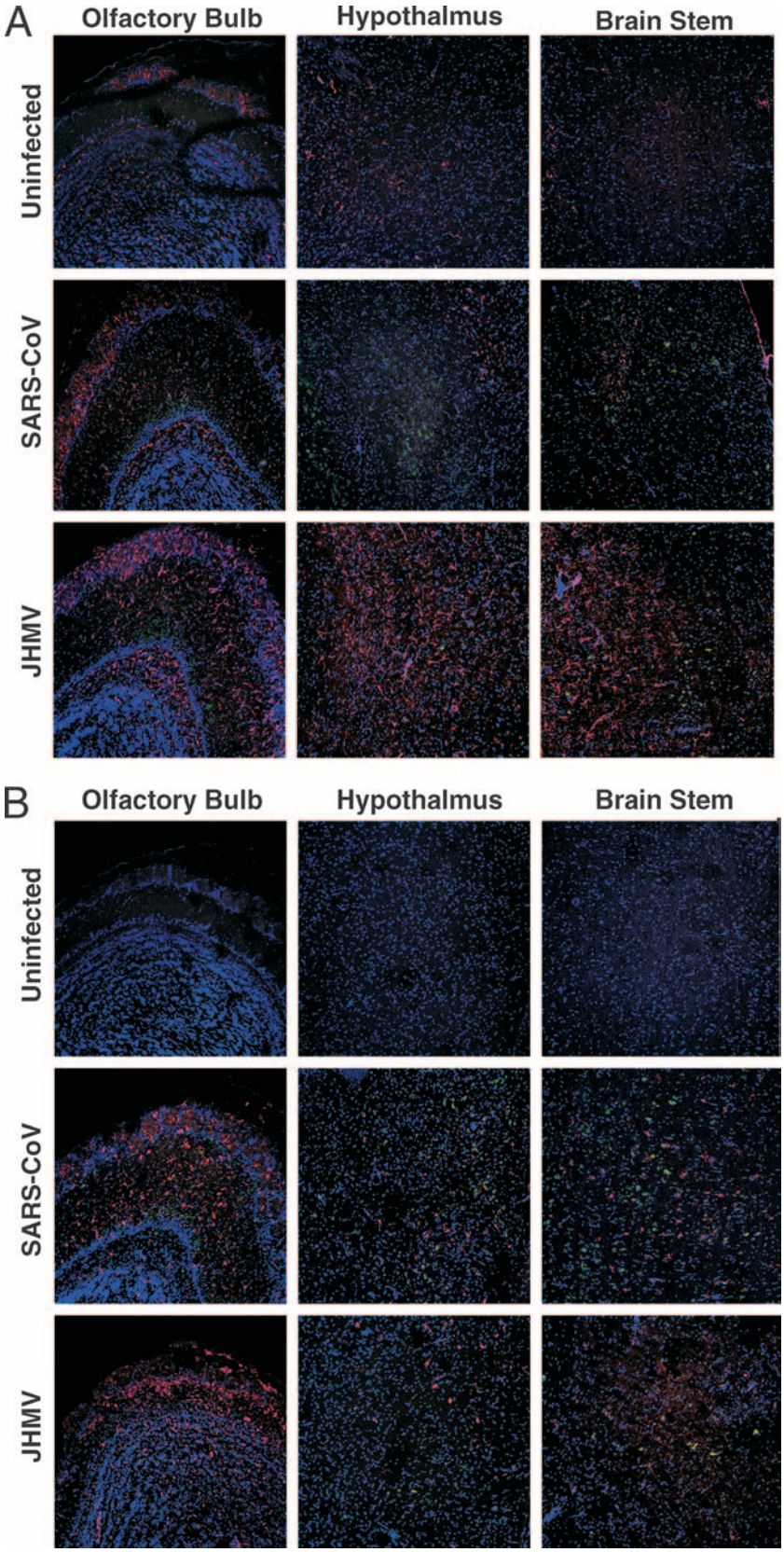

FIG. 6. SARS-CoV infection induces increased numbers of activated microglia but not astrocytes. Brain sections from uninfected and SARS-CoV- and JHMV-infected mice at day 6 p.i. were stained for viral antigen (green) and GFAP (astrocytes) or Iba1 (microglia/macrophage) (red). Nuclei were labeled with TOPRO-3 (blue). (A) Limited GFAP labeling was detected in uninfected and SARS-CoV-infected brains, while numerous GFAP cells were found in JHMV-infected brains. (B) No Iba1 immunoreactivity was found in uninfected brains while Iba1-positive cells were present in both SARS-CoV- and JHMV-infected samples. Original magnification, ×10 for all images.

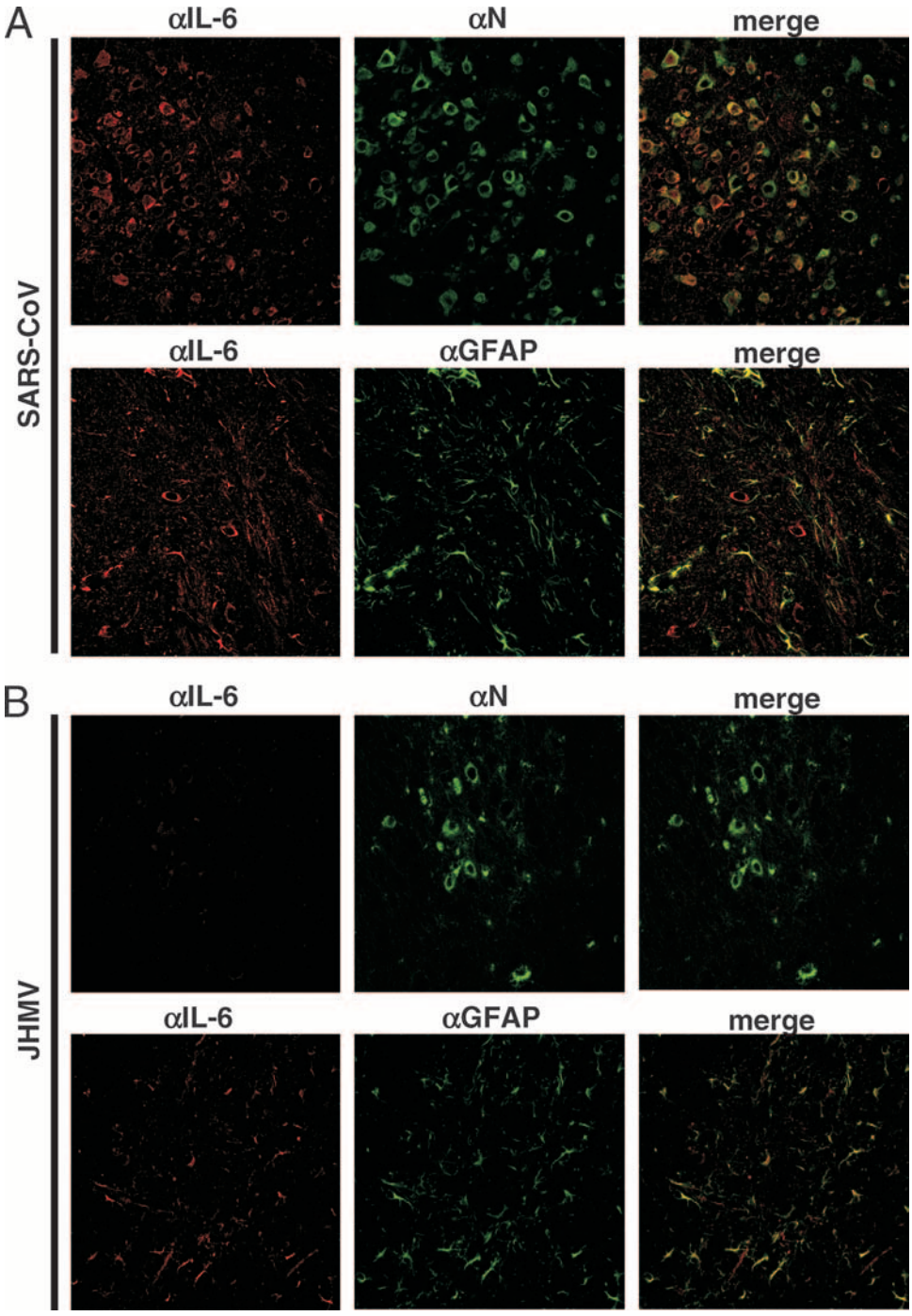

FIG. 7. IL-6 is expressed by SARS-CoV-infected but not JHMV-infected neurons. Brain sections were stained with anti-IL-6 antibody and either anti-SARS-CoV N, anti-JHMV N, or anti-GFAP antibody and analyzed by confocal microscopy. (A) In SARS-CoV-infected brains at 4 days p.i., IL-6 is expressed mostly by infected neurons but also by GFAP-positive astrocytes. (B) In JHMV-infected brains, most infected neurons do not express IL-6, and the majority of IL-6-positive cells are astrocytes. Images of SARS-CoV-infected brain depict the cortex. Images of JHMV-infected brain depict the midbrain (top row) and medulla (bottom row). Original magnification, ×40 for all images.

well established that excessive production of cytokines can lead to harmful effects in the brain and other tissues (reviewed in reference 2). An excessive and possibly dysregulated cytokine response has been implicated in neuronal death and death of the animal in an experimental model of Japanese encephalitis virus infection (18) and has also been implicated in patients with SARS (8, 10, 36). Lending support to this hypothesis, three cytokines often associated with immunopathology, IL-1β, tumor necrosis factor alpha, and IL-6 (2, 17, 30), are all upregulated in the brains of infected K18-*hACE2* mice (32). IL-6 was produced primarily by infected neurons (Fig. 7A). Neuronal production of IL-6 is not unprecedented, as neurons

expressing IL-6 have been detected in the developing brain (17), as well as in the adult hamster brain following ischemia (48). Furthermore, while murine neurons cultured in vitro constitutively express IL-6, expression can be substantially upregulated by infection with *Toxoplasma gondii* (41). However, neuronal production of IL-6 in vivo following viral infection has never been reported prior to our study to our knowledge. How SARS-CoV infection induces neurons to produce IL-6 is unknown. SARS-CoV products, such as the N protein, may directly induce IL-6 (55). Alternatively, IL-6 production may be a normal consequence of a highly productive neuronal infection or may be induced by another inflammatory mediator, such as IL-1β or tumor necrosis factor alpha (51), also expressed in the SARS-CoV-infected CNS (32).

Given this high-level expression of proinflammatory mediators, the lack of inflammation that we observe in the CNS is surprising and requires further investigation. SARS-CoV infects dendritic cells, at least in vitro (27, 43, 50, 56). Whether this occurs in vivo and interferes with initiation of the immune response is not known at present but may be one mechanism that would result in a diminished inflammatory response. It is also striking that we detected no evidence of apoptosis (Fig. 5B). Cells that die by necrosis would be expected to induce an immune response, but this was not detected in the SARS-CoV-infected CNS (Fig. 4G and H). Thus, another form of noninflammatory cell death, such as autophagy, may be involved in neuronal loss in SARS-CoV-infected K18-*hACE2* mice. Future experiments will be directed at examining this possibility.

Overall, these studies demonstrate a critical role for infection of the CNS in severe disease in SARS-CoV-infected K18-*hACE2* mice. Future studies will be directed to determining the mechanisms, both host and viral, by which SARS-CoV induces neuronal death and death of the animal. As SARS-CoV has been detected in the human CNS, studies of infected K18-*hACE2* mice may provide important insight into the pathogenesis of SARS in humans.

ACKNOWLEDGMENTS

We thank Noah Butler for careful review of the manuscript. We thank Lecia Pewe for technical advice and assistance.

This research was supported in part by a grant from the NIHI (PO1 AI060699). J.N. was supported by an NIH training grant (Training in Molecular Virology and Viral Pathogenesis T32 AI007533).

REFERENCES

1. **Akashi, H., Y. Inaba, Y. Miura, K. Sato, S. Tokuhisa, M. Asagi, and Y. Hayashi.** 1981. Propagation of the Kakegawa strain of bovine coronavirus in suckling mice, rats and hamsters. Arch. Virol. **67:**367–370.
2. **Allan, S. M., and N. J. Rothwell.** 2001. Cytokines and acute neurodegeneration. Nat. Rev. Neurosci. **2:**734–744.
3. **Aloisi, F.** 2001. Immune function of microglia. Glia **36:**165–179.
4. **Arbour, N., R. Day, J. Newcombe, and P. J. Talbot.** 2000. Neuroinvasion by human respiratory coronaviruses. J. Virol. **74:**8913–8921.
5. **Astic, L., D. Saucier, P. Coulon, F. Lafay, and A. Flamand.** 1993. The CVS strain of rabies virus as transneuronal tracer in the olfactory system of mice. Brain Res. **619:**146–156.
6. **Barnett, E. M., and S. Perlman.** 1993. The olfactory nerve and not the trigeminal nerve is the major site of CNS entry for mouse hepatitis virus, strain JHM. Virology **194:**185–191.
7. **Butler, N., L. Pewe, K. Trandem, and S. Perlman.** 2006. Murine encephalitis caused by HCoV-OC43, a human coronavirus with broad species specificity, is partly immune-mediated. Virology **347:**410–421.
8. **Cameron, M. J., L. Ran, L. Xu, A. Danesh, J. F. Bermejo-Martin, C. M. Cameron, M. P. Muller, W. L. Gold, S. E. Richardson, S. M. Poutanen, B. M. Willey, M. E. DeVries, Y. Fang, C. Seneviratne, S. E. Bosinger, D. Persad, P. Wilkinson, L. D. Greller, R. Somogyi, A. Humar, S. Keshavjee, M. Louie, M. B. Loeb, J. Brunton, A. J. McGeer, and D. J. Kelvin.** 2007. Interferon-mediated immunopathological events are associated with atypical innate and adaptive immune responses in patients with severe acute respiratory syndrome. J. Virol. **81:**8692–8706.
9. **Campbell, I. L., A. K. Stalder, C. S. Chiang, R. Bellinger, C. J. Heyser, S. Steffensen, E. Masliah, H. C. Powell, L. H. Gold, S. J. Henriksen, and G. R. Siggins.** 1997. Transgenic models to assess the pathogenic actions of cytokines in the central nervous system. Mol. Psychiatry **2:**125–129.
10. **Chan, P. K., J. W. Tang, and D. S. Hui.** 2006. SARS: clinical presentation, transmission, pathogenesis and treatment options. Clin. Sci. (Lond.) **110:**193–204.
11. **Cheng, S. K., J. S. Tsang, K. H. Ku, C. W. Wong, and Y. K. Ng.** 2004. Psychiatric complications in patients with severe acute respiratory syndrome (SARS) during the acute treatment phase: a series of 10 cases. Br. J. Psychiatry **184:**359–360.
12. **Coggeshall, R. E., and K. Chung.** 1984. The determination of an empirical correction factor to deal with the problem of nucleolar splitting in neuronal counts. J. Neurosci. Methods **10:**149–155.
13. **Couderc, T., F. Chretien, C. Schilte, O. Disson, M. Brigitte, F. Guivel-Benhassine, Y. Touret, G. Barau, N. Cayet, I. Schuffenecker, P. Despres, F. Arenzana-Seisdedos, A. Michault, M. L. Albert, and M. Lecuit.** 2008. A mouse model for chikungunya: young age and inefficient type-I interferon signaling are risk factors for severe disease. PLoS. Pathog. **4:**e29.
14. **Ding, Y., L. He, Q. Zhang, Z. Huang, X. Che, J. Hou, H. Wang, H. Shen, L. Qiu, Z. Li, J. Geng, J. Cai, H. Han, X. Li, W. Kang, D. Weng, P. Liang, and S. Jiang.** 2004. Organ distribution of severe acute respiratory syndrome (SARS) associated coronavirus (SARS-CoV) in SARS patients: implications for pathogenesis and virus transmission pathways. J. Pathol. **203:**622–630.
15. **Dong, Y., and E. N. Benveniste.** 2001. Immune function of astrocytes. Glia **36:**180–190.
16. **Drosten, C., S. Gunther, W. Preiser, S. van der Werf, H. R. Brodt, S. Becker, H. Rabenau, M. Panning, L. Kolesnikova, R. A. Fouchier, A. Berger, A. M. Burguiere, J. Cinatl, M. Eickmann, N. Escriou, K. Grywna, S. Kramme, J. C. Manuguerra, S. Muller, V. Rickerts, M. Sturmer, S. Vieth, H. D. Klenk, A. D. Osterhaus, H. Schmitz, and H. W. Doerr.** 2003. Identification of a novel coronavirus in patients with severe acute respiratory syndrome. N. Engl. J. Med. **348:**1967–1976.
17. **Gadient, R. A., and U. H. Otten.** 1997. Interleukin-6 (IL-6)—a molecule with both beneficial and destructive potentials. Prog. Neurobiol. **52:**379–390.
18. **Ghoshal, A., S. Das, S. Ghosh, M. K. Mishra, V. Sharma, P. Koli, E. Sen, and A. Basu.** 2007. Proinflammatory mediators released by activated microglia induces neuronal death in Japanese encephalitis. Glia **55:**483–496.
19. **Glass, W. G., K. Subbarao, B. Murphy, and P. M. Murphy.** 2004. Mechanisms of host defense following severe acute respiratory syndrome-coronavirus (SARS-CoV) pulmonary infection of mice. J. Immunol. **173:**4030–4039.
20. **Gu, J., E. Gong, B. Zhang, J. Zheng, Z. Gao, Y. Zhong, W. Zou, J. Zhan, S. Wang, Z. Xie, H. Zhuang, B. Wu, H. Zhong, H. Shao, W. Fang, D. Gao, F. Pei, X. Li, Z. He, D. Xu, X. Shi, V. M. Anderson, and A. S. Leong.** 2005. Multiple organ infection and the pathogenesis of SARS. J. Exp. Med. **202:**415–424.
21. **Harmer, D., M. Gilbert, R. Borman, and K. L. Clark.** 2002. Quantitative mRNA expression profiling of ACE 2, a novel homologue of angiotensin converting enzyme. FEBS Lett. **532:**107–110.
22. **Jacomy, H., and P. J. Talbot.** 2001. Susceptibility of murine CNS to OC43 infection. Adv. Exp. Med. Biol. **494:**101–107.
23. **Kim, T. S., and S. Perlman.** 2005. Virus-specific antibody, in the absence of T cells, mediates demyelination in mice infected with a neurotropic coronavirus. Am. J. Pathol. **166:**801–809.
24. **Ksiazek, T. G., D. Erdman, C. S. Goldsmith, S. R. Zaki, T. Peret, S. Emery, S. Tong, C. Urbani, J. A. Comer, W. Lim, P. E. Rollin, S. F. Dowell, A. E. Ling, C. D. Humphrey, W. J. Shieh, J. Guarner, C. D. Paddock, P. Rota, B. Fields, J. DeRisi, J. Y. Yang, N. Cox, J. M. Hughes, J. W. LeDuc, W. J. Bellini, and L. J. Anderson.** 2003. A novel coronavirus associated with severe acute respiratory syndrome. N. Engl. J. Med. **348:**1953–1966.
25. **Lau, K. K., W. C. Yu, C. M. Chu, S. T. Lau, B. Sheng, and K. Y. Yuen.** 2004. Possible central nervous system infection by SARS coronavirus. Emerg. Infect. Dis. **10:**342–344.
26. **Lavi, E., P. S. Fishman, M. K. Highkin, and S. R. Weiss.** 1988. Limbic encephalitis after inhalation of a murine coronavirus. Lab. Investig. **58:**31–36.
27. **Law, H. K., C. Y. Cheung, H. Y. Ng, S. F. Sia, Y. O. Chan, W. Luk, J. M. Nicholls, J. S. Peiris, and Y. L. Lau.** 2005. Chemokine up-regulation in SARS-coronavirus-infected, monocyte-derived human dendritic cells. Blood **106:**2366–2374.
28. **Lee, D. T., Y. K. Wing, H. C. Leung, J. J. Sung, Y. K. Ng, G. C. Yiu, R. Y. Chen, and H. F. Chiu.** 2004. Factors associated with psychosis among patients with severe acute respiratory syndrome: a case-control study. Clin. Infect. Dis. **39:**1247–1249.
29. **Li, W., M. J. Moore, N. Vasilieva, J. Sui, S. K. Wong, M. A. Berne, M. Somasundaran, J. L. Sullivan, K. Luzuriaga, T. C. Greenough, H. Choe, and M. Farzan.** 2003. Angiotensin-converting enzyme 2 is a functional receptor for the SARS coronavirus. Nature **426:**450–454.

30. **Lokensgard, J. R., M. C. Cheeran, S. Hu, G. Gekker, and P. K. Peterson.** 2002. Glial cell responses to herpesvirus infections: role in defense and immunopathogenesis. J. Infect. Dis. **186**(Suppl. 2)**:**S171—S179.
31. **Matthews, A. E., S. R. Weiss, and Y. Paterson.** 2002. Murine hepatitis virus—a model for virus-induced CNS demyelination. J. Neurovirol. **8:**76–85.
32. **McCray, P. B., Jr., L. Pewe, C. Wohlford-Lenane, M. Hickey, L. Manzel, L. Shi, J. Netland, H. P. Jia, C. Halabi, C. D. Sigmund, D. K. Meyerholz, P. Kirby, D. C. Look, and S. Perlman.** 2007. Lethal infection of K18-hACE2 mice infected with severe acute respiratory syndrome coronavirus. J. Virol. **81:**813–821.
33. **Ng, M. L., S. H. Tan, E. E. See, E. E. Ooi, and A. E. Ling.** 2003. Proliferative growth of SARS coronavirus in Vero E6 cells. J. Gen. Virol. **84:**3291–3303.
34. **Pavelko, K. D., C. L. Howe, K. M. Drescher, J. D. Gamez, A. J. Johnson, T. Wei, R. M. Ransohoff, and M. Rodriguez.** 2003. Interleukin-6 protects anterior horn neurons from lethal virus-induced injury. J. Neurosci. **23:**481–492.
34a. **Paxinos, G., and K. B. J. Franklin.** 2001. The mouse brain in stereotaxic coordinates, 2nd ed. Academic Press, New York, NY.
35. **Peiris, J. S., S. T. Lai, L. L. Poon, Y. Guan, L. Y. Yam, W. Lim, J. Nicholls, W. K. Yee, W. W. Yan, M. T. Cheung, V. C. Cheng, K. H. Chan, D. N. Tsang, R. W. Yung, T. K. Ng, and K. Y. Yuen.** 2003. Coronavirus as a possible cause of severe acute respiratory syndrome. Lancet **361:**1319–1325.
36. **Perlman, S., and A. A. Dandekar.** 2005. Immunopathogenesis of coronavirus infections: implications for SARS. Nat. Rev. Immunol. **5:**917–927.
37. **Plakhov, I. V., E. E. Arlund, C. Aoki, and C. S. Reiss.** 1995. The earliest events in vesicular stomatitis virus infection of the murine olfactory neuroepithelium and entry of the central nervous system. Virology **209:**257–262.
38. **Roberts, A., D. Deming, C. D. Paddock, A. Cheng, B. Yount, L. Vogel, B. D. Herman, T. Sheahan, M. Heise, G. L. Genrich, S. R. Zaki, R. Baric, and K. Subbarao.** 2007. A mouse-adapted SARS-coronavirus causes disease and mortality in BALB/c mice. PLoS Pathog. **3:**e5.
39. **Roberts, A., J. Wood, K. Subbarao, M. Ferguson, D. Wood, and T. Cherian.** 2006. Animal models and antibody assays for evaluating candidate SARS vaccines: summary of a technical meeting 25–26 August 2005, London, UK. Vaccine **24:**7056–7065.
40. **Rota, P. A., M. S. Oberste, S. S. Monroe, W. A. Nix, R. Campagnoli, J. P. Icenogle, S. Penaranda, B. Bankamp, K. Maher, M. H. Chen, S. Tong, A. Tamin, L. Lowe, M. Frace, J. L. DeRisi, Q. Chen, D. Wang, D. D. Erdman, T. C. Peret, C. Burns, T. G. Ksiazek, P. E. Rollin, A. Sanchez, S. Liffick, B. Holloway, J. Limor, K. McCaustland, M. Olsen-Rasmussen, R. Fouchier, S. Gunther, A. D. Osterhaus, C. Drosten, M. A. Pallansch, L. J. Anderson, and W. J. Bellini.** 2003. Characterization of a novel coronavirus associated with severe acute respiratory syndrome. Science **300:**1394–1399.
41. **Schluter, D., M. Deckert, H. Hof, and K. Frei.** 2001. *Toxoplasma gondii* infection of neurons induces neuronal cytokine and chemokine production, but gamma interferon- and tumor necrosis factor-stimulated neurons fail to inhibit the invasion and growth of *T. gondii*. Infect. Immun. **69:**7889–7893.
42. **Sharafeldin, A., R. Eltayeb, M. Pashenkov, and M. Bakhiet.** 2000. Chemokines are produced in the brain early during the course of experimental African trypanosomiasis. J. Neuroimmunol. **103:**165–170.
43. **Spiegel, M., K. Schneider, F. Weber, M. Weidmann, and F. T. Hufert.** 2006. Interaction of severe acute respiratory syndrome-associated coronavirus with dendritic cells. J. Gen. Virol. **87:**1953–1960.
44. **Stertz, S., M. Reichelt, M. Spiegel, T. Kuri, L. Martinez-Sobrido, A. Garcia-Sastre, F. Weber, and G. Kochs.** 2007. The intracellular sites of early replication and budding of SARS-coronavirus. Virology **361:**304–315.
45. **Stockman, L. J., R. Bellamy, and P. Garner.** 2006. SARS: systematic review of treatment effects. PLoS Med. **3:**e343.
46. **Subbarao, K., and A. Roberts.** 2006. Is there an ideal animal model for SARS? Trends Microbiol. **14:**299–303.
47. **Sun, N., D. Grzybicki, R. F. Castro, S. Murphy, and S. Perlman.** 1995. Activation of astrocytes in the spinal cord of mice chronically infected with a neurotropic coronavirus. Virology **213:**482–493.
48. **Suzuki, S., K. Tanaka, E. Nagata, D. Ito, T. Dembo, and Y. Fukuuchi.** 1999. Cerebral neurons express interleukin-6 after transient forebrain ischemia in gerbils. Neurosci. Lett. **262:**117–120.
49. **Tseng, C. T., C. Huang, P. Newman, N. Wang, K. Narayanan, D. M. Watts, S. Makino, M. M. Packard, S. R. Zaki, T. S. Chan, and C. J. Peters.** 2007. Severe acute respiratory syndrome coronavirus infection of mice transgenic for the human angiotensin-converting enzyme 2 virus receptor. J. Virol. **81:**1162–1173.
50. **Tseng, C. T., L. A. Perrone, H. Zhu, S. Makino, and C. J. Peters.** 2005. Severe acute respiratory syndrome and the innate immune responses: modulation of effector cell function without productive infection. J. Immunol. **174:**7977–7985.
51. **Van Wagoner, N. J., J. W. Oh, P. Repovic, and E. N. Benveniste.** 1999. Interleukin-6 (IL-6) production by astrocytes: autocrine regulation by IL-6 and the soluble IL-6 receptor. J. Neurosci. **19:**5236–5244.
52. **Wehn, S. M., E. R. Heinz, P. C. Burger, and O. B. Boyko.** 1989. Dilated Virchow-Robin spaces in cryptococcal meningitis associated with AIDS: CT and MR findings. J. Comput. Assist. Tomogr. **13:**756–762.
53. **Xu, J., S. Zhong, J. Liu, L. Li, Y. Li, X. Wu, Z. Li, P. Deng, J. Zhang, N. Zhong, Y. Ding, and Y. Jiang.** 2005. Detection of severe acute respiratory syndrome coronavirus in the brain: potential role of the chemokine mig in pathogenesis. Clin. Infect. Dis. **41:**1089–1096.
54. **Yamashita, M., M. Yamate, G. M. Li, and K. Ikuta.** 2005. Susceptibility of human and rat neural cell lines to infection by SARS-coronavirus. Biochem. Biophys. Res. Commun. **334:**79–85.
55. **Zhang, X., K. Wu, D. Wang, X. Yue, D. Song, Y. Zhu, and J. Wu.** 2007. Nucleocapsid protein of SARS-CoV activates interleukin-6 expression through cellular transcription factor NF-κB. Virology **365:**324–335.
56. **Ziegler, T., S. Matikainen, E. Ronkko, P. Osterlund, M. Sillanpaa, J. Siren, R. Fagerlund, M. Immonen, K. Melen, and I. Julkunen.** 2005. Severe acute respiratory syndrome coronavirus fails to activate cytokine-mediated innate immune responses in cultured human monocyte-derived dendritic cells. J. Virol. **79:**13800–13805.